Journal of
Composites Science

MDPI

Article

A C-Doped TiO_2/Fe_3O_4 Nanocomposite for Photocatalytic Dye Degradation under Natural Sunlight Irradiation

Mamo Gebrezgiabher [1], Gebrehiwot Gebreslassie [1], Tesfay Gebretsadik [1], Gebretinsae Yeabyo [2], Fikre Elemo [1], Yosef Bayeh [1], Madhu Thomas [1,*] and Wolfgang Linert [3]

1 Department of Industrial Chemistry, College of Applied Sciences, Addis Ababa Science and Technology University, P.O. Box 16417 Addis Ababa, Ethiopia
2 Department Chemistry, College of Natural and Computational Sciences, Mekelle University, P.O. Box 231 Mekelle, Ethiopia
3 Institute of Applied Synthetic Chemistry, Vienna University of Technology, Getreidemarkt 9/163-AC, A-1060 Vienna, Austria
* Correspondence: madhu.thomas@aastu.edu.et

Received: 11 June 2019; Accepted: 16 July 2019; Published: 22 July 2019

Abstract: Magnetically recyclable C-doped TiO_2/Fe_3O_4 (C-TiO_2/Fe_3O_4) nanocomposite was successfully synthesized via a sol–gel method. The synthesized samples were characterized using SEM, energy-dispersive X-ray spectroscopy (EDS), FTIR, and UV-VIS diffuse reflectance spectroscopy (DRS) techniques. The results clearly showed that a C-TiO_2/Fe_3O_4 nanocomposite was produced. The photocatalytic activities of the prepared pristine (TiO_2), C-doped TiO_2 (C-TiO_2) and C-TiO_2/Fe_3O_4 were evaluated by the photodegradation of methyl orange (MO) under natural sunlight. The effect of catalyst loading and MO concentration were studied and optimized. The C-TiO_2/Fe_3O_4 nanocomposite exhibited an excellent photocatalytic activity (99.68%) that was higher than the TiO_2 (55.41%) and C-TiO_2 (70%) photocatalysts within 150 min. The magnetic nanocomposite could be easily recovered from the treated solution by applying external magnetic field. The C-TiO_2/Fe_3O_4 composite showed excellent photocatalytic performance for four consecutive photocatalytic reactions. Thus, this work could provide a simple method for the mass production of highly photoactive and stable C-TiO_2/Fe_3O_4 photocatalyst for environmental remediation.

Keywords: photodegradation; C-TiO_2/Fe_3O_4 nanocomposite; natural sunlight; dye degradation

1. Introduction

Recently, TiO_2-based photocatalysts have been used in several applications, such as antimicrobial activity [1], water splitting [2], hydrogen production [3], carbon dioxide reduction [4], organic pollutant degradation [5–8], solar cells [9–11], batteries [12], and super capacitors [13,14]. Currently, the search has intensified for an abundant, inexpensive, efficient, safe, and recyclable photocatalyst that can be used for degradation of organic contaminants, for instance, methyl orange (MO) in wastewater treatment and/or water purification. Over the last decade, scientific research interest for developing such a photocatalyst has been growing exponentially [6,15–19]. Among the reported photocatalysts, TiO_2-based photocatalysts seem to be more popular because of their chemical stability, strong oxidizing power, nontoxicity, and low cost [20–22]. However, there are still some drawbacks that need to be addressed for this type of photocatalyst. For example, its band gap (i.e., 3.2 eV) only absorbs UV light at less than 388 nm. Therefore, several strategies have been developed to enhance the optical absorption of TiO_2, such as colorant sensitization, metal- or nonmetal-doped TiO_2-based nanoparticles

(NPs), and modification of TiO_2 by combining it with another metal oxide-based semiconductor [23]. In addition to this, TiO_2 NPs are difficult to recover from treated water, which results in the discharge of TiO_2 NPs into the environment. One alternative solution to this problem is to apply an NP photocatalyst that is immobilized on a permanent magnetic carrier, which permits it to be recollected from the treated water using an external magnetic field and then reused again. Immobilization of photocatalytic TiO_2 NPs on magnetic transporter can be done by sol–gel method [24], plasma spraying [25], and precipitation [26].

Magnetic photocatalysts are a more attractive and economical method of water treatment for the future because they are capable of treating a large volume of wastewater with a small amount of magnetic photocatalyst over its useable lifespan, which is impossible with conventional purification methods. Iron oxides are the most common magnetic materials, which are cheap, easy to prepare, strongly magnetic, and environmentally benign [27,28]. Extensive efforts have been made to combine TiO_2 photocatalyst with magnetic iron oxide NPs as a feasible strategy to build an effectively stable and easily recoverable composite photocatalyst [29–31]. Over the past few years, a number of TiO_2-based hybrid photocatalysts with iron oxide-based magnetic materials have been reported, such as TiO_2/Fe_3O_4 [32,33], $Ag_3PO_4/TiO_2/Fe_3O_4$ [34], Ni–Zn–ferrite/TiO_2 [35], and N-doped $TiO_2/ZnFe_2O_4$ [36], to improve photocatalytic activity, cycling stability, and long-term durability in the photodegradation of dye pollutants. However, the magnetic properties and photodissolution of magnetic iron oxides happen upon direct deposition with the active photocatalysts, which reduces the photocatalytic activity of the photocatalyst [37].

Here, we synthesized a C-TiO_2/Fe_3O_4 nanocomposite via a sol–gel method and characterized it using several characterization techniques, such as XRD, SEM, energy-dispersive spectroscopy (EDS), FTIR, and UV-VIS diffuse reflectance spectroscopy (DRS). The photocatalytic activity of the as-prepared pristine and nanocomposites were evaluated for MO (Scheme 1) degradation under natural sunlight. The C-TiO_2/Fe_3O_4 nanocomposite photocatalyst showed better photocatalytic activity than the TiO_2 and C-TiO_2 photocatalysts. Therefore, the prepared nanocomposite photocatalyst would exhibit enhanced photocatalytic activity under natural sunlight with excellent stability and recyclability.

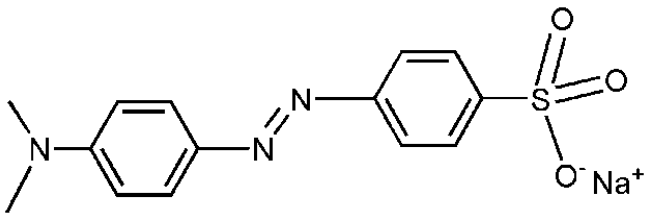

Scheme 1. Structure of methyl orange.

2. Experimental Part

2.1. Chemicals

Hydrochloric acid, methyl orange, ethanol, titanium chloride, ammonia, glucose, iron(II)chloridetetrahydrate, and iron(III)chloridehexahydrate were purchased from Merck, (Mumbai, India). All the chemicals were of analytical grade and used without any purification. Distilled water was used in all the experiments.

2.2. Synthesis of Photocatalysts

TiO_2 NPs were prepared using a sol–gel method. Twenty milliliters of the precursor $TiCl_3$ was added to 180 mL of distilled water. The mixed solution was stirred vigorously for 30 min. Then, 2 M ammonia aqueous solution was added drop-wise to the above solution with simultaneous stirring until a white precipitate was observed. Thereafter, the obtained precipitate was washed repeatedly until no chloride was detected in the filtrate. The precipitate was dried in an oven at 200 °C for 3 h, calcined at 450 °C for 1 h, cooled to room temperature, and stored in a moisture-free atmosphere

for the next step. C-TiO_2 photocatalyst was synthesized by mixing a stoichiometric amount of precursor and the desired amount of powdered glucose (99%) (i.e., C:Ti mole ratio of 1:6) [38]. These mixtures were then transported to muffle furnace and calcinated at 300 °C for 5 h. After natural cooling, C-TiO_2 photocatalysts were collected and kept for the next steps.

Fe_3O_4 was prepared using a titration coprecipitation approach [39]. One hundred milliliters of 0.15 mol/L $FeCl_3{\cdot}6H_2O$ aqueous solution and 200 mL of 0.15 mol/L $FeCl_2{\cdot}4H_2O$ aqueous solution were mixed in a three-necked flask. The mixed solution was stirred at 40 °C. Then, ammonia solution was dropped into the mixed solution until the pH value reached 9. After that, a large amount of black precipitate was produced. The obtained Fe_3O_4 precipitate was washed with distilled water and ethanol numerous times until the pH value reached 7. Lastly, the Fe_3O_4 was dried in an oven at 40 °C and collected.

C-TiO_2/Fe_3O_4 composite was synthesized using facile thermal sol–gel method. Typically, Fe_3O_4 (0.01 mol) was dispersed in the mixture solution of water–ethanol with a volume ratio of 1:20. After stirring the suspension for about 15 min using a magnetic stirrer, a diluted HCl aqueous solution was added into the suspension until the pH value of the mixture reached 5. Then, 6 mg of C-TiO_2 dissolved in 50 mL of distilled water was slowly dropped into the above suspension. The suspension was vigorously stirred for 30 min to ensure a uniform composition. The precipitates were recovered by magnetic separation and washed with ethanol and deionized water until the pH value reached 7. The nanocomposite was aged for 5 h and then dried in open air oven at 60 °C. Then, the prepared C-TiO_2/Fe_3O_4 composite was calcined at 450 °C for 3 h.

2.3. Characterization Techniques

The following were used as characterization techniques: XRD (Shimadzu Corp., Kyoto, Japan, operating at 40 kV and 30 mA, using Cu Kα radiation (1.5406 Å), step scan mode with step time and degree (2θ) of 0.4 s and 0.02°, respectively, for the range of 10° to 80°); UV-VIS DRS (Perkin Elmer Lamda 35 spectrometer (PerkinElmer, Inc., Waltham, MA, USA), at a wavelength range of 200–800 nm); FTIR spectrophotometer (IR prestige 21 (Shimadzu Corp.), in the range of 400–4000 cm^{-1} using KBr pellets); SEM (INSPECT^{TM} F50, FEI Company, Hillsboro, OR, USA); and EDS equipped with SEM (JEOL JSM-5610 SEM, JEOL, Ltd., Tokyo, Japan).

2.4. Photocatalytic Activity

The photocatalytic activity of the prepared pristine and nanocomposite photocatalysts were studied for the degradation of MO under natural sunlight irradiation. Typically, the photocatalytic degradation experiments were carried out by adding 20 mg photocatalyst to MO dye aqueous solution (5 mg/L, 100 mL sample volume) in a 500 mL beaker (Scheme 2). Then, the mixture was stirred for 1 h in a dark place to obtain absorption–desorption equilibrium. The mixed solution was then exposed to natural sunlight. To significantly minimize the fluctuation of sunlight intensity, all photodegradation experiments were carried out around midday (between 11 a.m. to 2 p.m.) in the same month (December, 2018) and in the same place (Addis Ababa, Ethiopia). Thereafter, a 3 mL sample was taken at every 30 min interval of sunlight irradiation. The magnetic photocatalysts were separated using a magnet, and nonmagnetic photocatalysts were separated using a centrifuge. The residual concentration of MO was analyzed by the change in absorbance using a UV-VIS spectrophotometer (Optizen POP, Mecasys Co., Ltd, Daejeon, Korea) at 464 nm (λ_{max} of MO). The effect of the catalyst dose was studied by varying the amount of photocatalyst loading from 10 to 50 mg by keeping the MO concentration (5 mg/L, 100 mL) and other parameters constant. The effect of the initial dye concentration was examined by varying the concentration of MO from 5 to 25 mg/L, keeping the catalyst dose at 20 mg in 100 mL volume of MO solution, with other parameters remaining constant.

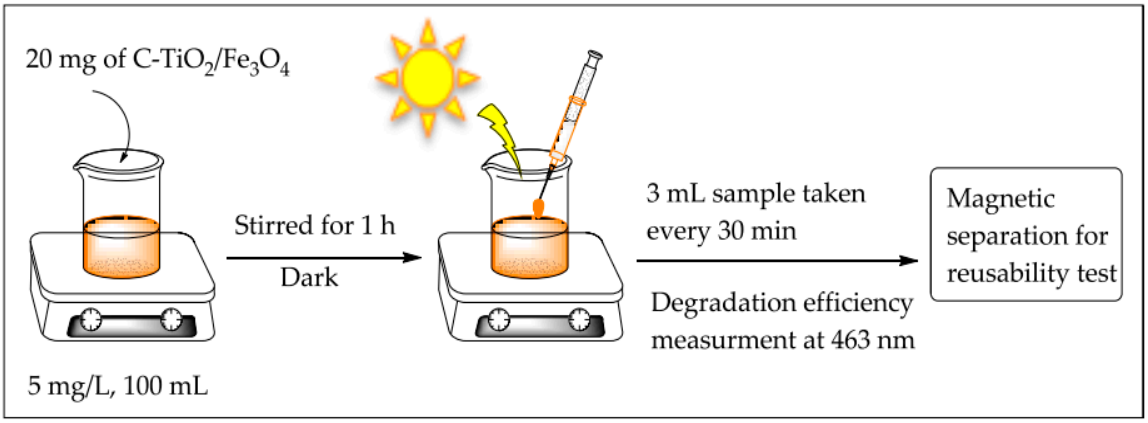

Scheme 2. Schematic illustration for the photocatalytic degradation of methyl orange (MO).

3. Results and Discussion

3.1. Characterization Results

The morphology of pristine and nanocomposite samples was investigated by XRD. Figure 1a shows the XRD patterns of TiO_2, C-TiO_2, Fe_3O_4, and C-TiO_2/Fe_3O_4 nanocomposites. The XRD peak at 35.6° is a characteristic peak of magnetic phase of Fe_3O_4 [40]. The XRD peaks corresponding to Fe_3O_4 clearly resembled the standard diffraction pattern of magnetite (JCPDS file No. 03-0863). The average crystallite size of the as-prepared Fe_3O_4 powder, as estimated by the Scherrer formula, was around 14 nm from the (311) peak, which showed the as-prepared particles were in the nanosize range [41]. There were no diffraction peaks of carbon in the C-TiO_2/Fe_3O_4 nanocomposites due to their amorphous nature and low content compared to Fe_3O_4 and TiO_2. In addition to all diffraction peaks of Fe_3O_4, four other diffraction peaks appeared at 2θ = 25.3°, 37.8°, 48.1°, 55.1°, and 63.5°, which corresponded to (101), (004), (200), and (211) planes of anatase TiO_2 (JCPDS file No. 21-1272), respectively, in the C-TiO_2/Fe_3O_4 nanocomposites. XRD results demonstrated that the crystalline anatase TiO_2 and Fe_3O_4 coexisted in the C-TiO_2/Fe_3O_4 sample. It could be observed that the intensity of the Fe_3O_4 peak decreased after being combined with TiO_2. This reduction might be due to the effect of the TiO_2 layer coating on Fe_3O_4 NPs.

The FTIR spectra of the synthesized samples (Figure 1b) showed broad bands in the range 3200–3460 cm^{-1}, associated with the stretching vibration of the –OH species [32,42]. In addition, peaks at about 1650 cm^{-1} were related to the H–OH bending of the adsorbed water molecules [42]. The FTIR spectrum of TiO_2 showed a broad characteristic peak of Ti–O–Ti vibration at 500–900 cm^{-1} [32,42], while a strong absorption band of Fe–O stretching vibration at 600 cm^{-1} [42–44] was clearly observed. Strong OH stretching frequency suggested high intensity of surface hydroxide, which enabled better dispersion of Fe_3O_4 nanoparticles and also enhanced the affinity between Fe_3O_4 nanoparticles and the precursor TiO_2 [32]. The characteristic peaks of both C-TiO_2 and Fe_3O_4 were noticed in the spectrum (Figure 1b), suggesting that the C-TiO_2/Fe_3O_4 nanocomposite was successfully prepared.

The morphologies of TiO_2, Fe_3O_4, C-TiO_2, and C-TiO_2/Fe_3O_4 samples were examined using SEM and are presented in Figure 2. Figure 2a displays the SEM image of the TiO_2 nanoparticles in which many nearly monodispersed spheres could be seen. The surfaces of the TiO_2 spheres were rough. Figure 2b shows the SEM image of the Fe_3O_4 spherically shaped colloidal particles. As shown in Figure 2c, agglomerated C-TiO_2 could be observed. This might be due to the carbon matrix doped on the TiO_2 spheres. Figure 2d is the SEM image of the C-TiO_2/Fe_3O_4 nanocomposite, where many tiny C-TiO_2 nanoparticles were adhered to the Fe_3O_4. The surfaces of the C-TiO_2/Fe_3O_4 nanocomposites were smooth, which was distinctly different from the initial C-TiO_2 spheres that are shown in Figure 2c. Such a difference can be attributed to the loading of C-TiO_2 on Fe_3O_4. Furthermore, the elemental analysis of TiO_2, C-TiO_2, and C-TiO_2/Fe_3O_4 samples were investigated using EDS, and the images are

displayed in Figure 3. The EDS peaks of TiO_2 samples were ascribed to Ti and O elements, as shown in Figure 3a. For the C-TiO_2 sample, the peaks were associated with C, Ti, and O elements (Figure 3b). As shown in Figure 3c, C, Ti, Fe, and O elements were present in the EDS spectra of C-TiO_2/Fe_3O_4 nanocomposites. Hence, we can conclude that TiO_2, C-TiO_2, and C-TiO_2/Fe_3O_4 nanocomposite samples were prepared successfully.

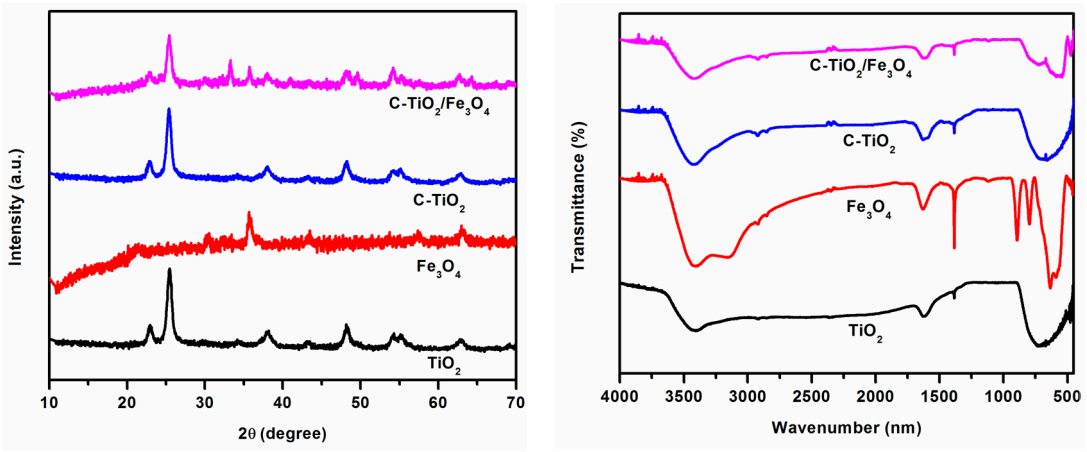

(**a**) (**b**)

Figure 1. (**a**) XRD pattern of TiO_2, Fe_3O_4, C-TiO_2, and C-TiO_2/Fe_3O_4 nanocomposites and (**b**) FTIR spectra of TiO_2, Fe_3O_4, C-TiO_2, and C-TiO_2/Fe_3O_4 composites.

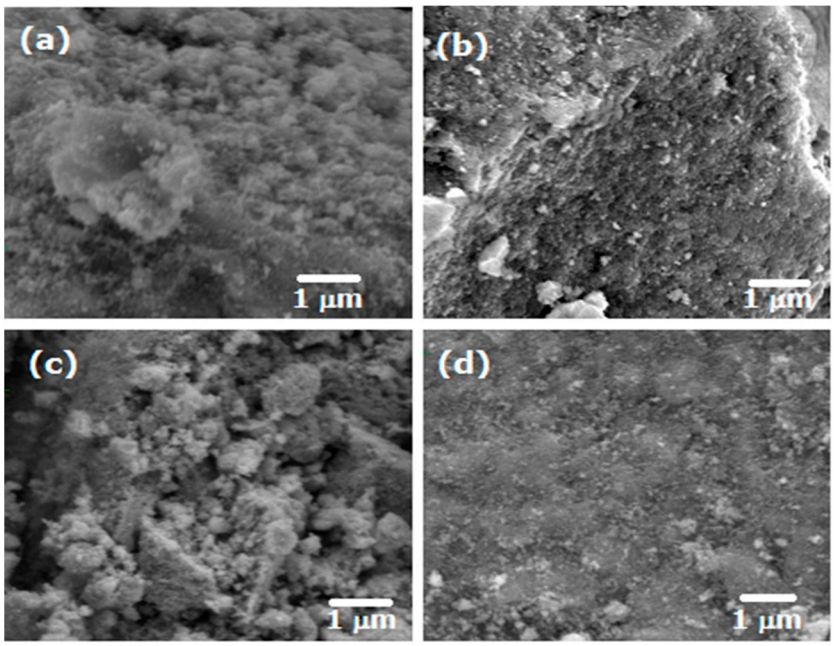

Figure 2. SEM images of (**a**) TiO_2, (**b**) Fe_3O_4, (**c**) C-doped TiO_2, and (**d**) C-doped TiO_2/Fe_3O_4 nanocomposites.

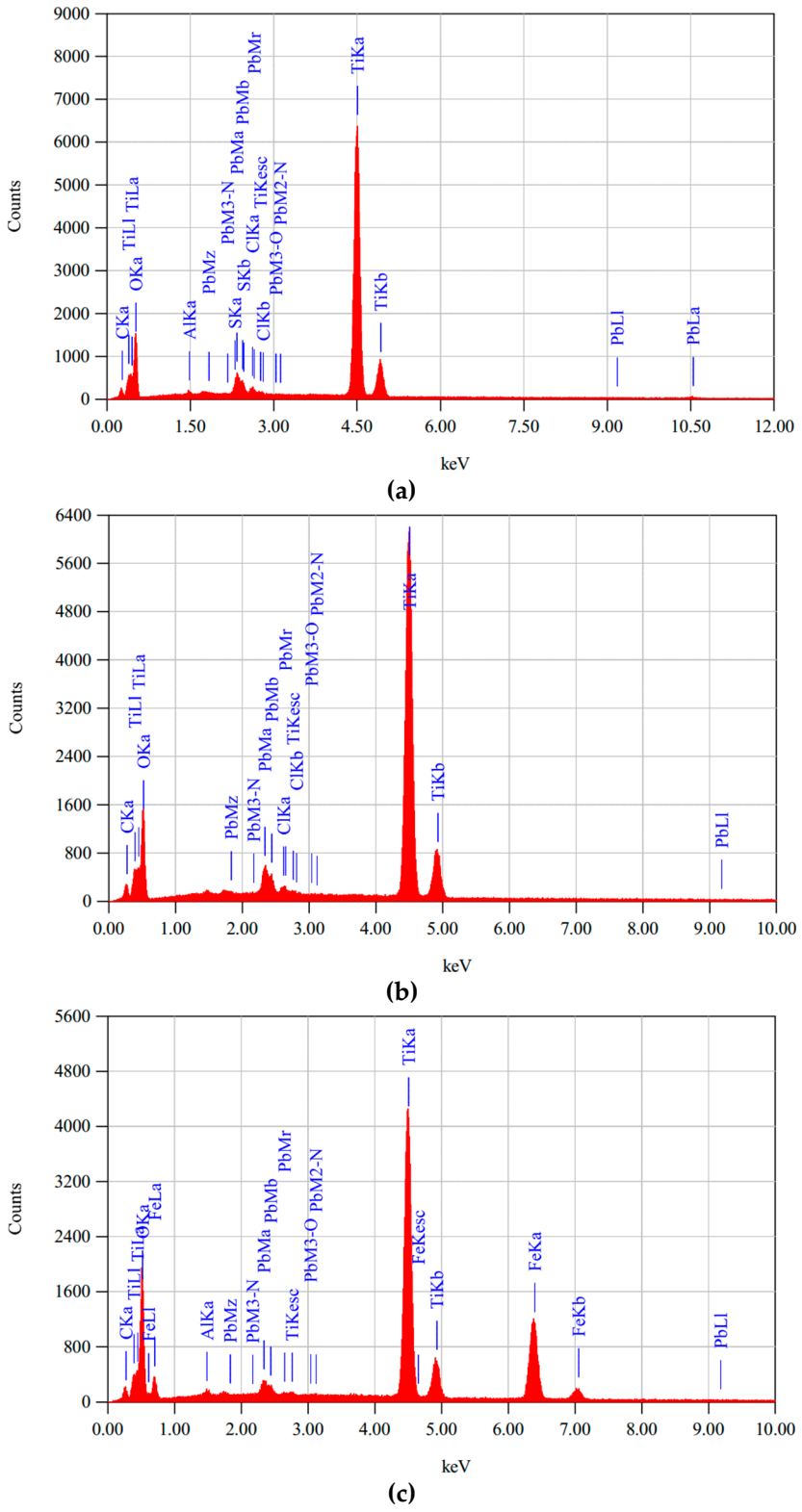

Figure 3. Energy-dispersive spectroscopy (EDS) images of (**a**) TiO_2 (**b**) C-TiO_2, and (**c**) C-TiO_2/Fe_3O_4 samples.

The optical properties of the photocatalysts were studied using UV-VIS DRS, and the results for TiO_2, C-TiO_2, and C-TiO_2/Fe_3O_4 nanocomposites are given in Figure 4a. It shows that the absorption edge of TiO_2 was 375 nm and that it could only be absorbed in the UV region. After doping of TiO_2 by carbon, its optical response shifted into the visible region. The UV-VIS DRS spectra demonstrated that

the C-TiO_2/Fe_3O_4 material could adsorb significantly more light in the 200–800 nm regions compared to TiO_2 and C-TiO_2 materials. As a result, it was found that the C-TiO_2/Fe_3O_4 nanocomposite showed better photocatalytic activity in the visible light region than TiO_2 and C-TiO_2. Moreover, the band gap energy (Eg) of the as-prepared samples were estimated using Tauc's equation [45] by extrapolation of the linear part of the curves obtained by plotting of (α hv)2 vs. hv. As shown in Figure 4b, the Eg values of pure TiO_2, C-TiO_2, and C-TiO_2/Fe_3O_4 samples were 3.0, 2.5, and 2.4 eV, respectively. As a result, the C-TiO_2/Fe_3O_4 nanocomposite exhibited an enhanced absorption in the visible region compared to the pure TiO_2 and C-TiO_2 photocatalyst.

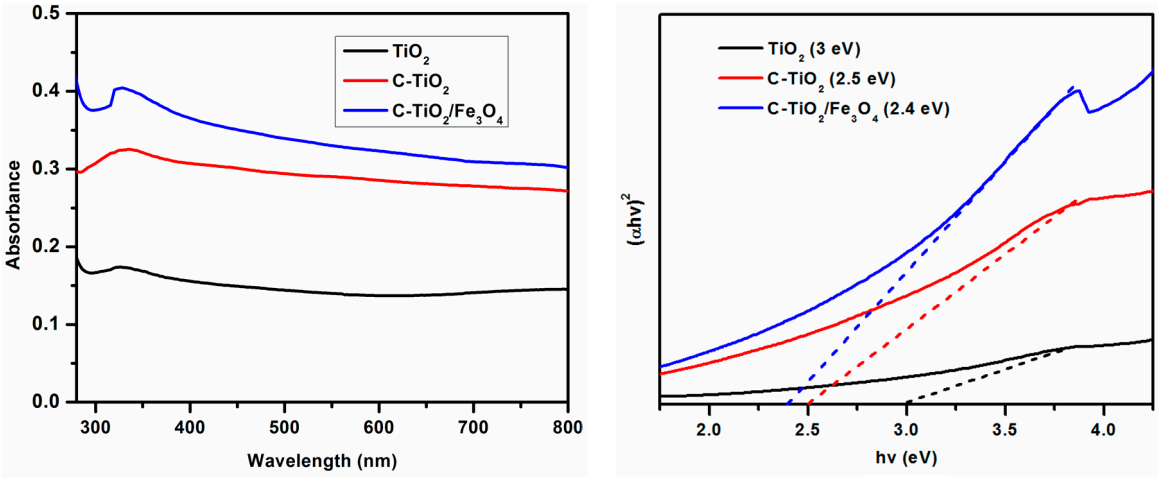

Figure 4. (**a**) UV-VIS diffuse reflectance spectra (DRS) of TiO_2, C-TiO_2, and C-TiO_2/Fe_3O_4 composite and (**b**) (α hv)2 vs. hv curve of TiO_2, C-TiO_2, and C-TiO_2/Fe_3O_4 photocatalysts.

3.2. Photocatalytic Activity

The photocatalytic degradation rate of the MO pollutant depends on the MO concentration and dose of the photocatalyst. As shown in Figure 5a, the degradation efficiency decreased as concentration of MO increased from 5 to 25 mg/L at constant catalyst dose (20 mg/100 mL). Therefore, the initial concentration of MO was taken to be 5 mg/L. Furthermore, Figure 5b shows the effect of photocatalyst loading on the degradation efficiency at constant MO concentration (100 mL, 5 mg/L). When the amount of photocatalyst loading increased from 10 to 20 mg, the degradation efficiency was enhanced. However, as the catalyst dose increased from 20 to 50 mg, the degradation efficiency decreased. Therefore, the optimum photocatalyst dose was found to be 20 mg/L.

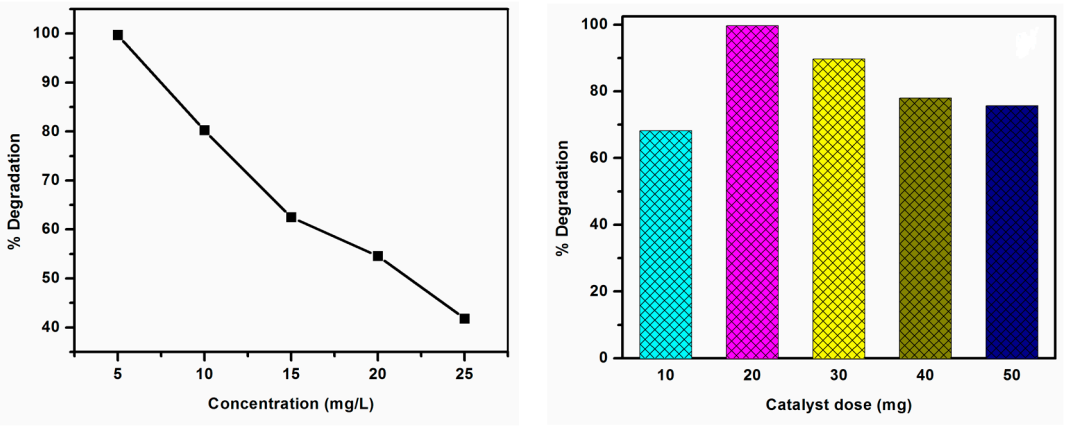

Figure 5. Effect of (**a**) initial dye concentration and (**b**) catalyst dosage on the photodegradation efficiency.

After optimizing the MO concentration (5 mg/L) and catalyst dose (20 mg/L), the photocatalytic activity of TiO_2, C-TiO_2, and C-TiO_2/Fe_3O_4 materials were investigated for MO degradation under solar light irradiation. The C-TiO_2/Fe_3O_4 nanocomposite showed higher photocatalytic activity than TiO_2 and C-TiO_2 samples (Figure 6a). The C-TiO_2/Fe_3O_4 nanocomposite degraded 99.68% of MO pollutant within 150 min, while the TiO_2 and C-TiO_2 degraded about 55.41% and 70%, respectively. This could be due to the fast electron-hole separation and low-rate photogenerated electron-hole recombination in the nanocomposite than in the TiO_2 and C-TiO_2 samples. Photocatalyst recyclability is very important in practical application. For this reason, the C-TiO_2/Fe_3O_4 nanocomposite was recovered using external magnetic field and reused for photodegradation reactions after being washed and dried. As shown in Figure 6b, the C-TiO_2/Fe_3O_4 nanocomposite showed almost the same photocatalytic performance for four consecutive photocatalytic reactions, indicating the nanocomposite photocatalyst has excellent photocatalytic stability.

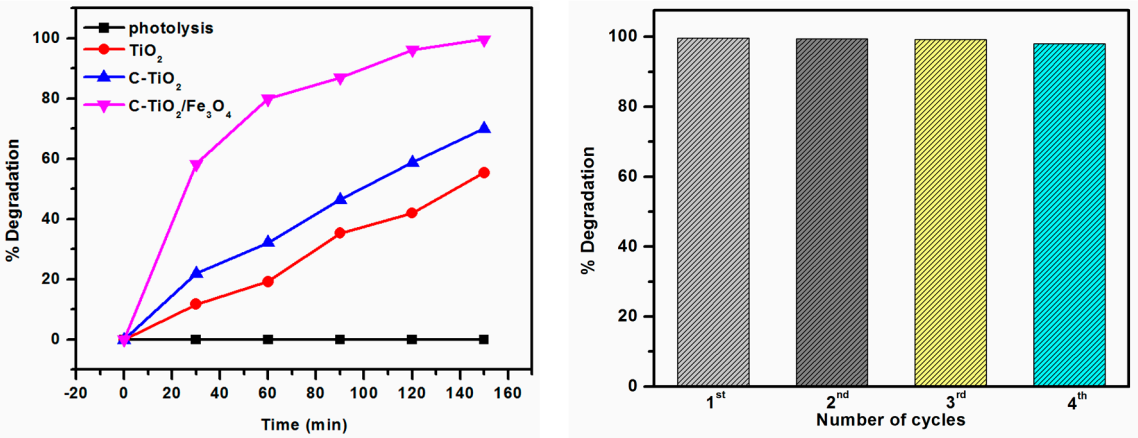

Figure 6. (**a**) Photolysis of MO and photocatalytic degradation of MO over pure TiO_2, C-TiO_2, and C-TiO_2/Fe_3O_4 photocatalysts and (**b**) recyclability study of C-TiO_2/Fe_3O_4 nanocomposite photocatalyst.

We also compared the photocatalyst efficiency of the synthesized C-TiO_2/Fe_3O_4 nanocomposite with previous TiO_2-based studies (Table 1). As shown, the C-TiO_2/Fe_3O_4 nanocomposite prepared here showed excellent photocatalytic activity compared to the previous works.

Table 1. Comparison of photocatalytic activities of some selected nanocomposites with the present work.

Catalyst	Preparation Method	Catalyst Load (mg/mL)	Pollutant Load (mg/L)	Type of Pollutant	Light Source	% Degradation	Ref.
Fe_3O_4/TiO_2	Solvothermal	0.3	10	Natural red	30 W Xenon	100% in 120 min	[32]
Fe_3O_4 /TiO_2	Emulsion copolymerization	0.4	5	Rhodamine B	250 W Hg	100% in 120 min	[33]
Fe_3O_4/TiO_2	Chemical coprecipitation	0.1	20	Methyl blue	10 W LED	90% in 300 min	[40]
N-TiO_2/$ZnFe_2O_4$	Vapor–thermal	0.4	5	Rhodamine B	500 W Hg	100% in 240 min	[36]
C-TiO_2/Fe_3O_4	Sol–gel	0.2	5	Methyl orange	Natural sunlight	99.68% in 150 min	This work

4. Conclusions

A visible-light photoactive and magnetically separable C-TiO_2/Fe_3O_4 nanocomposite was successfully prepared by facile sol–gel method and fully characterized in its crystal structure, optical properties, and morphologies. The photocatalytic activity of the prepared pristine and nanocomposite

catalysts were investigated for MO degradation under natural sunlight irradiation. The C-TiO_2/Fe_3O_4 nanocomposite showed higher catalytic activity than TiO_2 and C-TiO_2. The enhancement in the photodegradation efficiency could be attributed to the synergistic effect of C-TiO_2 and Fe_3O_4 components. In addition, it could be easily separated using external magnetic field and showed excellent photocatalyst stability for four consecutive cycles.

Author Contributions: All the authors participated in conceptualizing, executing, analyzing and writing the original draft except the last two authors (M.T. and W.L.) who were responsible for supervision, editing, and reviewing of this article.

Funding: This research project was supported by the Internal Research grant of Addis Ababa Science and Technology University (Project/Reference Number: IRG 02/09).

Acknowledgments: The authors are grateful to Addis Ababa Science and Technology University for providing necessary facilities for this work.

Conflicts of Interest: The authors declare no conflict of interest.

References

1. Nguyen, V.T.; Vu, V.T.; Nguyen, T.H.; Nguyen, T.A.; Tran, V.K.; Nguyen-Tri, P. Antibacterial Activity of TiO_2- and ZnO-Decorated with Silver Nanoparticles. *J. Compos. Sci.* **2019**, *3*, 61. [CrossRef]
2. Miyoshi, A.; Nishioka, S.; Maeda, K. Water Splitting on Rutile TiO_2-Based Photocatalysts. *Chem. A Eur. J.* **2018**, *24*, 18204–18219. [CrossRef] [PubMed]
3. Guayaquil-Sosa, J.F.; Calzada, A.; Serrano, B.; Escobedo, S.; de Lasa, H. Hydrogen Production via Water Dissociation Using Pt–TiO_2 Photocatalysts: An Oxidation–Reduction Network. *Catalysts* **2017**, *7*, 324. [CrossRef]
4. Shehzad, N.; Tahir, M.; Johari, K.; Murugesan, T.; Hussain, M. A Critical Review on TiO_2 Based Photocatalytic CO_2 Reduction System: Strategies to Improve Efficiency. *J. CO2 Util.* **2018**, *26*, 98–122. [CrossRef]
5. Mekassa, B.; Tessema, M.; Chandravanshi, B.S.; Tefera, M. Square Wave Voltammetric Determination of Ibuprofen at Poly(L-Aspartic Acid) Modified Glassy Carbon Electrode. *IEEE Sens. J.* **2018**, *18*, 37–44. [CrossRef]
6. Gebreslassie, G.; Bharali, P.; Chandra, U.; Sergawie, A.; Boruah, P.K.; Das, M.R.; Alemayehu, E. Hydrothermal Synthesis of G-C_3N_4/$NiFe_2O_4$ Nanocomposite and Its Enhanced Photocatalytic Activity. *Appl. Organomet. Chem.* **2019**, e5002.
7. Sun, M.; Senthil, R.; Pan, J.; Osman, S.; Khan, A. A Facile Synthesis of Visible-Light Driven Rod-on-Rod like α-FeOOH/α-$AgVO_3$ Nanocomposite as Greatly Enhanced Photocatalyst for Degradation of Rhodamine B. *Catalysts* **2018**, *8*, 392. [CrossRef]
8. Thao, L.T.S.; Dang, T.T.T.; Khanitchaidecha, W.; Channei, D.; Nakaruk, A. Photocatalytic Degradation of Organic Dye under UV-A Irradiation Using TiO_2-Vetiver Multifunctional Nano Particles. *Materials* **2017**, *10*, 122. [CrossRef] [PubMed]
9. Sacco, A.; Bella, F.; De La Pierre, S.; Castellino, M.; Bianco, S.; Bongiovanni, R.; Pirri, C.F. Electrodes/Electrolyte Interfaces in the Presence of a Surface-Modified Photopolymer Electrolyte: Application in Dye-Sensitized Solar Cells. *ChemPhysChem* **2015**, *16*, 960–969. [CrossRef]
10. Bella, F.; Galliano, S.; Piana, G.; Giacona, G.; Viscardi, G.; Grätzel, M.; Barolo, C.; Gerbaldi, C. Boosting the Efficiency of Aqueous Solar Cells: A Photoelectrochemical Estimation on the Effectiveness of $TiCl_4$ Treatment. *Electrochim. Acta* **2019**, *302*, 31–37. [CrossRef]
11. Bella, F.; Verna, A.; Gerbaldi, C. Patterning Dye-Sensitized Solar Cell Photoanodes through a Polymeric Approach: A Perspective. *Mater. Sci. Semicond. Process.* **2018**, *73*, 92–98. [CrossRef]
12. Bella, F.; Muñoz-García, A.B.; Colò, F.; Meligrana, G.; Lamberti, A.; Destro, M.; Pavone, M.; Gerbaldi, C. Combined Structural, Chemometric, and Electrochemical Investigation of Vertically Aligned TiO_2 Nanotubes for Na-Ion Batteries. *ACS Omega* **2018**, *3*, 8440–8450. [CrossRef]
13. Jiang, L.; Luo, D.; Zhang, Q.; Ma, S.; Wan, G.; Lu, X.; Ren, Z. Electrochemical Performance of Free-Standing and Flexible Graphene and TiO_2 Composites with Different Conductive Polymers as Electrodes for Supercapacitors. *Chem. A Eur. J.* **2019**, *25*, 7903–7911. [CrossRef] [PubMed]

14. Yang, S.; Li, Y.; Sun, J.; Cao, B. Laser Induced Oxygen-Deficient TiO_2/Graphene Hybrid for High-Performance Supercapacitor. *J. Power Sources* **2019**, *431*, 220–225. [CrossRef]
15. Ansari, S.A.; Khan, M.M.; Ansari, M.O.; Cho, M.H. Nitrogen-Doped Titanium Dioxide (N-Doped TiO_2) for Visible Light Photocatalysis. *New J. Chem.* **2016**, *40*, 3000–3009. [CrossRef]
16. Babu, S.G.; Karthik, P.; John, M.C.; Lakhera, S.K.; Ashokkumar, M.; Khim, J.; Neppolian, B. Synergistic Effect of Sono-Photocatalytic Process for the Degradation of Organic Pollutants Using CuO-TiO_2/RGO. *Ultrason. Sonochem.* **2019**, *50*, 218–223. [CrossRef]
17. Rizzo, L.; Sannino, D.; Vaiano, V.; Sacco, O.; Scarpa, A.; Pietrogiacomi, D. Effect of Solar Simulated N-Doped TiO_2 Photocatalysis on the Inactivation and Antibiotic Resistance of an E. Coli Strain in Biologically Treated Urban Wastewater. *Appl. Catal. B Environ.* **2014**, *144*, 369–378. [CrossRef]
18. Fu, J.; Zhu, B.; You, W.; Jaroniec, M.; Yu, J. A Flexible Bio-Inspired H_2-Production Photocatalyst. *Appl. Catal. B Environ.* **2018**, *220*, 148–160. [CrossRef]
19. Zhang, L.; Zhang, Q.; Xie, H.; Guo, J.; Lyu, H.; Li, Y.; Sun, Z.; Wang, H.; Guo, Z. Electrospun Titania Nanofibers Segregated by Graphene Oxide for Improved Visible Light Photocatalysis. *Appl. Catal. B Environ.* **2017**, *201*, 470–478. [CrossRef]
20. Moreira, N.F.F.; Sousa, J.M.; Macedo, G.; Ribeiro, A.R.; Barreiros, L.; Pedrosa, M.; Faria, J.L.; Pereira, M.F.R.; Castro-Silva, S.; Segundo, M.A.; et al. Photocatalytic Ozonation of Urban Wastewater and Surface Water Using Immobilized TiO_2 with LEDs: Micropollutants, Antibiotic Resistance Genes and Estrogenic Activity. *Water Res.* **2016**, *94*, 10–22. [CrossRef]
21. Moreira, N.F.F.; Narciso-da-Rocha, C.; Polo-López, M.I.; Pastrana-Martínez, L.M.; Faria, J.L.; Manaia, C.M.; Fernández-Ibáñez, P.; Nunes, O.C.; Silva, A.M.T. Solar Treatment (H_2O_2, TiO_2-P25 and GO-TiO_2 Photocatalysis, Photo-Fenton) of Organic Micropollutants, Human Pathogen Indicators, Antibiotic Resistant Bacteria and Related Genes in Urban Wastewater. *Water Res.* **2018**, *135*, 195–206. [CrossRef] [PubMed]
22. Qin, N.; Xiong, J.; Liang, R.; Liu, Y.; Zhang, S.; Li, Y.; Li, Z.; Wu, L. Highly Efficient Photocatalytic H_2 Evolution over MoS_2/CdS-TiO_2 Nanofibers Prepared by an Electrospinning Mediated Photodeposition Method. *Appl. Catal. B Environ.* **2017**, *202*, 374–380. [CrossRef]
23. Zanjanchi, M.A.; Noei, H.; Moghimi, M. Rapid Determination of Aluminum by UV-Vis Diffuse Reflectance Spectroscopy with Application of Suitable Adsorbents. *Talanta* **2006**, *70*, 933–939. [CrossRef] [PubMed]
24. Álvarez, P.M.; Jaramillo, J.; López-Piñero, F.; Plucinski, P.K. Preparation and Characterization of Magnetic TiO_2 Nanoparticles and Their Utilization for the Degradation of Emerging Pollutants in Water. *Appl. Catal. B Environ.* **2010**, *100*, 338–345. [CrossRef]
25. Yu, Q.; Zhou, C.; Wang, X. Influence of Plasma Spraying Parameter on Microstructure and Photocatalytic Properties of Nanostructured TiO_2-Fe_3O_4 Coating. *J. Mol. Catal. A Chem.* **2008**, *283*, 23–28. [CrossRef]
26. He, Q.; Zhang, Z.; Xiong, J.; Xiong, Y.; Xiao, H. A Novel Biomaterial—Fe_3O_4:TiO_2 Core-Shell Nano Particle with Magnetic Performance and High Visible Light Photocatalytic Activity. *Opt. Mater.* **2008**, *31*, 380–384. [CrossRef]
27. Tai, Y.; Wang, L.; Yan, G.; Gao, J.M.; Yu, H.; Zhang, L. Recent Research Progress on the Preparation and Application of Magnetic Nanospheres. *Polym. Int.* **2011**, *60*, 976–994. [CrossRef]
28. Wu, W.; He, Q.; Jiang, C. Magnetic Iron Oxide Nanoparticles: Synthesis and Surface Functionalization Strategies. *Nanoscale Res. Lett.* **2008**, *3*, 397–415. [CrossRef]
29. Amarjargal, A.; Jiang, Z.; Tijing, L.D.; Park, C.H.; Im, I.T.; Kim, C.S. Nanosheet-Based α-Fe_2O_3 Hierarchical Structure Decorated with TiO_2 Nanospheres via a Simple One-Pot Route: Magnetically Recyclable Photocatalysts. *J. Alloys Compd.* **2013**, *580*, 143–147. [CrossRef]
30. Li, X.; Niu, C.; Huang, D.; Wang, X.; Zhang, X.; Zeng, G.; Niu, Q. Preparation of Magnetically Separable Fe_3O_4/BiOI Nanocomposites and Its Visible Photocatalytic Activity. *Appl. Surf. Sci.* **2013**, *286*, 40–46. [CrossRef]
31. Liu, R.; Wu, C.F.; Ger, M.D. Degradation of FBL Dye Wastewater by Magnetic Photocatalysts from Scraps. *J. Nanomater.* **2015**, *16*, 168. [CrossRef]
32. Niu, H.; Wang, Q.; Liang, H.; Chen, M.; Mao, C.; Song, J.; Zhang, S.; Gao, Y.; Chen, C. Visible-Light Active and Magnetically Recyclable Nanocomposites for the Degradation of Organic Dye. *Materials* **2014**, *7*, 4034–4044. [CrossRef] [PubMed]
33. Xuan, S.; Jiang, W.; Gong, X.; Hu, Y.; Chen, Z. Magnetically Separable Fe_3O_4/TiO_2 Hollow Spheres: Fabrication and Photocatalytic Activity. *J. Phys. Chem. C* **2009**, *113*, 553–558. [CrossRef]

34. Xu, J.-W.; Gao, Z.-D.; Han, K.; Liu, Y.; Song, Y.-Y. Synthesis of Magnetically Separable $Ag_3PO_4/TiO_2/Fe_3O_4$ Heterostructure with Enhanced Photocatalytic Performance under Visible Light for Photoinactivation of Bacteria. *ACS Appl. Mater. Interfaces* **2014**, *6*, 15122–15131. [CrossRef] [PubMed]
35. Liu, R.; Ou, H.T. Synthesis and Application of Magnetic Photocatalyst of Ni-Zn Ferrite/TiO_2 from IC Lead Frame Scraps. *J. Nanotechnol.* **2015**, *2015*, 727210. [CrossRef]
36. Yao, Y.; Qin, J.; Chen, H.; Wei, F.; Liu, X.; Wang, J.; Wang, S. One-Pot Approach for Synthesis of N-Doped $TiO_2/ZnFe_2O_4$ Hybrid as an Efficient Photocatalyst for Degradation of Aqueous Organic Pollutants. *J. Hazard. Mater.* **2015**, *291*, 28–37. [CrossRef] [PubMed]
37. Beydoun, D.; Amal, R.; Low, G.K.-C.; McEvoy, S. Novel Photocatalyst: Titania-Coated Magnetite. Activity and Photodissolution. *J. Phys. Chem. B* **2002**, *104*, 4387–4396. [CrossRef]
38. Rajkumar, R.; Nisha, S. To Study the Effect of the Concentration of Carbon on Ultraviolet and Visible Light Photo Catalytic Activity and Characterization of Carbon Doped TiO_2. *J. Nanomed. Nanotechnol.* **2015**, *6*, 1. [CrossRef]
39. Soo, K.Y.; Risbud, S.; Rabolt, J.F.; Stroeve, P. Synthesis and Characterization of Nanometer-Size Fe_3O_4 and γ-Fe_2O_3 Particles. *Chem. Mater.* **1996**, *8*, 2209–2211.
40. Tedsree, K.; Temnuch, N.; Sriplai, N.; Pinitsoontorn, S. Ag Modified Fe_3O_4@TiO_2 Magnetic Core-Shell Nanocomposites for Photocatalytic Degradation of Methylene Blue. *Mater. Today Proc.* **2017**, *4*, 6576–6584. [CrossRef]
41. Zhang, Q.; Zhu, M.; Zhang, Q.; Li, Y.; Wang, H. Fabrication and Magnetic Property Analysis of Monodisperse Manganese-Zinc Ferrite Nanospheres. *J. Magn. Magn. Mater.* **2009**, *321*, 3203–3206. [CrossRef]
42. Nakamoto, K. *Infrared and Raman Spectra of Inorganic and Coordination Compounds (Part A: Theory and Applications in Inorganic Chemistry)*, 6th ed.; Nakamoto, K., Ed.; John Wiley & Sons: Hoboken, NJ, USA, 2009.
43. Ghorbani-Choghamarani, A.; Darvishnejad, Z.; Tahmasbi, B. Schiff Base Complexes of Ni, Co, Cr, Cd and Zn Supported on Magnetic Nanoparticles: As Efficient and Recyclable Catalysts for the Oxidation of Sulfides and Oxidative Coupling of Thiols. *Inorg. Chim. Acta* **2015**, *435*, 223–231. [CrossRef]
44. Ghorbani-Choghamarani, A.; Norouzi, M. Palladium Supported on Modified Magnetic Nanoparticles: A Phosphine-Free and Heterogeneous Catalyst for Suzuki and Stille Reactions. *Appl. Organomet. Chem.* **2016**, *30*, 140–147. [CrossRef]
45. Guayaquil-Sosa, J.F.; Serrano-Rosales, B.; Valadés-Pelayo, P.J.; de Lasa, H. Photocatalytic Hydrogen Production Using Mesoporous TiO_2 Doped with Pt. *Appl. Catal. B Environ.* **2017**, *211*, 337–348. [CrossRef]